ISSN 1070-4272, Russian Journal of Applied Chemistry, 2018, Vol. 91, No. 2, pp. 235−244. © Pleiades Publishing, Ltd., 2018.

VARIOUS TECHNOLOGICAL PROCESSES

Sequential Dehydration and Oxidation of Biodiesel-derived Crude Glycerol into Acrylic Acid[1]

Lu Quanlin[a], Liu Rong[b,*], and Xia Guofan[c]

[a]*School of Environmental and Chemical Engineering, Shanghai University, Shanghai, 200444, China*
[b] *Huaneng Clean Energy Research Institute, Beijing 102209, China*
[c] *Beijing Institute of Architectural Design, Beijing 100045, China*
**e-mail: liurong@hnceri.com*

Received January 9, 2018

Abstract—With the fast development of the biodiesel industry, the byproduced crude glycerol becomes excessive due to the limited demand for refined glycerol. This article provides a green and efficient route to produce acrylic acid from crude glycerol, which is a promising alternative and complement to the petroleum-based production of acrylic acid due to its economic and environmental benefits. Among all the impurities, only the alkaline metal ions in crude glycerol significantly decreased the yield of acrylic acid. After desalination of the plant crude glycerol with ion-exchange resin to remove the critical impurities, the sequential dehydration and oxidation system gave 86% acrylic acid yield, which was as high as that with pure glycerol. In addition, the system showed good thermal stability and regeneration ability after the reaction with desalted crude glycerol. Both the HPW/Cs–Nb and VMo–SiC catalysts were stable for at least 70 h. The activity and selectivity were well recovered after regeneration at the coke burning temperature of 500°C.

DOI: 10.1134/S1070427218020118

INTRODUCTION

The development of renewable and alternative fuels such as biodiesel is becoming increasingly important because of the depletion of fossil fuels and global warming [1, 2]. Biodiesel is currently produced by transesterification of triglycerides and methanol, in which crude glycerol is produced as a main byproduct. Many studies have been reported on the utilization of glycerol by oxidation, hydrogenolysis, pyrolysis, transesterification, esterification, polymerization, and dehydration [3–5]. Among these, the sequential dehydration and oxidation of biodiesel-derived crude glycerol into acrylic acid is an attractive and promising process. Acrylic acid is widely used in polymer dispersions, adhesives, fibers, plastics, and other chemical intermediates [3, 4, 6].

Compared with refined glycerol, crude glycerol is much cheaper because it is very costly to remove all the impurities by bleaching, deodorizing, and ion exchange [7–10]. Nowadays, the price of refined glycerol is 900−1000 US$ per ton, while crude glycerol is available at only ~150 US$ per ton. This makes the sustainable production of acrylic acid from crude glycerol much more competitive compared with that from pure glycerol reported in previous work [11,12].

Crude glycerol from biodiesel production contains organic and inorganic impurities such as methanol, free fatty acids, alkli metal ions and soap. Its composition varies according to different oil feedstock and biodiesel production processes. The alkli metal ions are mainly from KOH or NaOH used as catalysts for transesterification to produce biodiesel [4, 13]. Typical crude glycerol from biodiesel plant using waste cooking oil as feedstock is dark brown viscous liquid, and contains only 27–60% glycerol [13, 14]. The impurities were methanol (6–10%), free fatty acid (1–7.5%), K^+ (4–5%), and water [13, 15, 16].

In this work, the feasibility of using crude glycerol as feedback for acrylic acid production by dehydration-oxidation reactions was investigated. The dehydration catalyst was $Cs_{2.5}H_{0.5}PW_{12}O_{40}$ supported on Nb_2O_5

[1] The text was submitted by the authors in English.

(CsPW–Nb). For the oxidation of acrolein to acrylic acid, many types of catalysts have been studied, among which the vanadium–molybdenum mixed oxides commercialized for the partial oxidation of propylene give the best catalytic performance. These two catalysts had very similar optimum reaction temperature and oxygen ratio. This made the two-bed system very simple and efficient. However, the use of this system in the conversion of crude glycerol to acrylic acid needs further experimental validation due to the change in the reactant composition. To make the new technology more commercially competitive, the efficient removal of the impurities that affects the dehydration-oxidation of glycerol to acrylic acid was investigated. The impurities had no influence on the commercialized oxidation catalyst, so the effects of different impurities on the dehydration catalyst were investigated in detail. The goal was to develop a pretreatment method to remove the critical impurities and achieve a high yield of acrylic acid directly from crude glycerol. The yield of acrylic acid was 85% after the removal of the critical impurities. The CsPW–Nb and VMo–SiC catalysts were stable for at least 70 h, and had very good thermal stability at coke burning temperature of 500°C.

EXPERIMENTAL

Catalyst preparation. *Introduction of Cs_2CO_3 and $H_3PW_{12}O_{40}$ and Nb_2O_5 by the vacuum-assisted impregnation method.* After being separated and dried, the Nb_2O_5 precipitates were pretreated under a vacuum of better than 0.1 Pa to remove the impurities and trapped air in the porous structure. The obtained Nb_2O_5 was not calcined before impregnation with Cs_2CO_3 and $H_3PW_{12}O_{40}$. A desired amount of Cs_2CO_3 was added to deionized water, and the 0.10 M Cs_2CO_3 solution of was added to mix with the Nb_2O_5 powder under vacuum. Then the vacuum was turned off and the system was kept overnight at atmospheric pressure and room temperature to let Cs_2CO_3 get into the micro- and mesopores of Nb_2O_5 by capillary force. Excess water was removed using a rotary evaporator at 40°C and dried at 100°C in air for 2 h. After the $H_3PW_{12}O_{40}$ was impregnated into the prepared Cs_2CO_3/Nb_2O_5 with the same procedure except the fact that a 0.08 M $H_3PW_{12}O_{40}$ solution was used. The powder after drying was heated in flowing air to 500°C at 5°C/min, calcined for 4 h and then cooled to room temperature at 5°C/min. According to the CsPW loading (*w* in wt %), the final catalyst samples were denoted as HPW/Cs–Nb.

Na-loaded HPW/Cs–Nb was prepared by impregnation. $NaNO_3 \cdot 9H_2O$ (Alfa Aesar) was used as the sodium ions source. The HPW/Cs–Nb precursor and $NaNO_3$ aqueous solution were mixed, stirred, and subsequently dried at 313 K for 2 h and then at 333 K for 2 h. The obtained precipitate was dried at 383 K for 24 h and finally calcined at 773 K for 2 h in an air atmosphere. The content of Na^+ was varied in the range of 0–10 wt % based on the total amount of HPW , denoted hereafter as *x*Na–HPW/Cs–Nb, where *x* was the Na content (wt %).

For the oxidation reaction, the vanadium–molybdenum oxide supported on the silicon carbide, denoted as VMo–SiC in this work, was synthesized by incipient wetness impregnation [21]. Firstly, 0.59 g ammonium metavanadate (NH_4VO_3, Alfa Aesar) and 3 g ammonium heptamolybdate ($(NH_4)_6Mo_7O_{24} \cdot 4H_2O$, Alfa Aesar) precursors were dissolved in 11.3 mL deionized water at 80°C. A solution of 0.33 g ammonium oxalato-niobate $Nb(NH_4)(C_2O_4)_2NbO \cdot nH_2O$ (Aldrich, 99.99%) was then added to this aqueous solution while stirring. An aqueous solution of 0.7 g copper sulfate ($CuSO_4$, Alfa Aesar) dissolved in 1 mL heated deionized water was added similarly. Antimony trioxide (Sb_2O_3, Alfa Aesar), 0.3 g, was added to the solution. The precursor solution was slowly dropped onto 8.5 g silicon carbide (SiC, 150 μm Alfa Aesar). The sample was dried at 80°C for 15 min, and was further dried at 100°C overnight. Finally, the catalysts were calcined at 380°C for 5 h with flowing air.

Characterization. The XRD analysis was performed on an automated powder X-ray diffractometer (40 kV, 40 mA, Bruke D8 Advance) using a CuK_α radiation source and a nickel filter in the 2θ range of 1–90°. The samples were dried under vacuum at 200°C for 5 h before measurement. In order to test the catalyst stability, the XRD results of the catalysts after calcination at 500°C in air were also analyzed for comparison.

NH_3-TPD was carried out using an automated adsorption system (ChemBET Pulsar TPR/TPD, Quantachrome) with an online thermal conductivity detector (TCD). A sample of 100 mg was placed in a quartz tubular reactor and pretreated at 150°C with a N_2 flow of 30 mL min^{-1} for 1 h, and then cooled to 100°C. NH_3 was introduced at a flow rate of 30 mL min^{-1} for 0.5 h at 100°C, and then the sample was purged in N_2 stream until a constant TCD level was obtained. The reactor temperature was programmed at a rate of 5°C/min to 700°C and the desorbed NH_3 was detected online by the TCD.

The acidic properties of the catalysts were characterized with FTIR spectroscopy using pyridine as probe molecule. The FTIR spectrometer (Nicolet NEXUS670) had a heatable IR cell with a KBr window connected to the gas dosing-evacuating system. The powder sample was pressed to self-supporting wafers (10 mm in diameter, 30 mg). The sample was pretreated in flowing Ar at 300°C for 1 h and then cooled to room temperature. Pyridine was adsorbed for 1 h by directing an Ar stream through a pyridine-containing saturator. Physically adsorbed pyridine was flushed away by evacuating for 5 min at room temperature. Pyridine desorption was carried out at 200°C under high vacuum conditions to accomplish complete desorption of physically adsorbed pyridine. The infrared spectra were recorded in transmission mode with 2 cm^{-1} resolution and 100 scans. A background correction was made by collecting the spectra without sample prior to the measurement.

The Na^+ and K^+ content in the solutions was analyzed by atomic absorption spectrophotometry with a Varian (Madrid, Spain) 220 AS spectrophotometer. The standard uncertainty and reproducibility of measurements were ±0.1%.

Catalytic reaction. Glycerol solution with different feed composition was used to study the effect of impurities. The aqueous solutions were prepared with pure glycerol ($C_3H_8O_3$, ultrapure, HPLC Grade, Alfa Aesar) or crude glycerol. Plant crude glycerol (pH = 11.4) was from a biodiesel pilot plant using NaOH or KOH as catalyst. The plant crude glycerol was filtered through a frit type S1 (porous size 110 nm) and then water was added to give the required concentration. The composition of diluted plant crude glycerol is shown in Table 1. The plant crude glycerol from alkaline transesterification process was mainly composed of glycerol, methanol, soap, free fatty acids (FFAs), fatty acid methyl ester (FAMEs), glycerides, and alkli metal ions. The synthetic crude glycerol contained one of the following impurities: methanol, FFA (linoleic acid), FAME (methyl oleate), glycerides (glycerol monostearate), Na^+ (NaCl) and K^+ (KCl). The weight percent of impurity in each synthetic crude glycerol was 5 wt %, which is relatively high compared with biodiesel-waste glycerol. The use of high impurity content allows to study the influence of impurities in a shorter reaction time. Desalted plant crude glycerol was also used as feedstock. Ion exchangers were used in the desalination process [17–21]. A commercial ion-exchange resin D001-CC provided by Tianjin Bohong Resin Technology Co. Ltd was used to remove the alkali metal ions. The D001-CC resins are of Na^+ type and were pretreated to H^+ type using the procedure described by Zheng et al [22]. Na^+ and K^+ were exchanged with protons initially on the resin until the resin exchange capacity was exhausted. The concentrations of glycerol and organic impurities in the treated solution were analyzed by gas chromatography equipped with an FID detector (GC–FID). The amount of Na^+ and K^+ were determined by atomic absorption spectrophotometry [23]. The final removal rate of the alkaline metal anions was 95% with 6% loss of glycerol, as listed in Table 1.

Table 1 The composition of plant crude and desalted glycerol

Samples		Plant crude glycerol	Desalted glycerol
Glycerol, wt %		21.50	20.20
Methanol, wt %		2.30	1.50
Glycerides, wt %	mono-	0.51	0.48
	di-	0.11	0.08
FAMEs, wt %	Palmitate	0.51	0.43
	Stearate	2.75	2.36
	Oleate	1.23	1.28
	Linoleate	2.36	2.25
Na^+, wt %		0.46	0.11
K^+, wt %		3.32	0.14

The experiments of dehydration–oxidation of glycerol to acrylic acid were carried out under ambient pressure in a fixed-bed reactor (10 mm i.d.). For the two-bed experiments, 0.5 g HPW/Cs–Nb was loaded in the top bed for glycerol dehydration, and 0.5 g VMo–SiC was loaded in the bottom bed for subsequent oxidation of acrolein. In addition to HPW/Cs–Nb, the Na-loaded catalysts Na^+–HPW/Cs–Nb were also used as dehydration to study the influence of alkali metal ions. The catalysts were diluted with inert quartz particles to avoid hot spots. The particle size of the catalysts was in the range of 325–500 μm. The reactor tube was placed in an electrical furnace with an inner diameter matching the outer diameter of the reactor tube to give a good heat transfer and a long zone of uniform temperature. A HPLC pump (Series 2,001-5 mL min^{-1}, SS, S. G. Seal Self Flush, Pulse Damper) was used to feed solution of 20 wt % glycerol from the top of the reactor. Dry nitrogen (15 mL min^{-1}) mixed with oxygen (3 mL min^{-1}) was used as carrier gas, and the flow rates were controlled by mass flow controllers.

The measured axial profile of the catalyst bed temperature confirmed that the reaction was carried out under isothermal conditions. All reactants and products in the tubings were heated to at least 200°C to avoid undesired condensation.

The reaction products and unconverted glycerol were collected in a cold trap (–5°C) at the reactor outlet. The collected liquids were analyzed offline by gas chromatograph (GC 7900, Techcomp Ltd.) equipped with a FID detector and a TM-Super Wax column (60 m × 0.25 mm × 0.25 μm, Techcomp Ltd). The mass balance for each trap was determined to confirm proper operation of the setup. The reaction was conducted for 30 h in most cases. The condensed products during the first two hours of reaction were not used because they did not satisfy the mass balance. The glycerol conversion and product selectivity were calculated based on the number of carbon atoms as follows:

$$\text{Glycerol conversion} = \frac{\text{Moles of reacted glycerol}}{\text{Moles of glycerol in the feed}} \times 100\%,$$

$$\text{Product selectivity} = \frac{\text{Moles of carbon in the defined product}}{\text{Moles of carbon in the reacted glycerol}} \times 100\%,$$

$$\text{Product yield} = \text{Glycerol yield} \times \text{Product selectivity}.$$

Glycerol has primary and secondary hydroxyl groups, it and also has two main reaction pathways for sequential dehydration and oxidation. Over the dehydration–oxidation system, acrylic acid was the main product. Trace amounts of methane, ethane, ethylene, propane, and propylene were also detected.

RESULTS AND DISCUSSION

Influence of Impurities on the Catalyst Properties

XRD patterns. The powder XRD patterns of fresh and used HPW/Cs-Nb are very similar, as shown in Fig. 1. No significant changes were observed from the XRD patterns of the catalysts after the dehydration reaction. The XRD patterns of HPW (Fig. 1a) presented the characteristic peaks corresponding to the Kegging anion [24]. The Na^+ partially substituted salts $Na_{0.5}H_{2.5}PW_{12}O_{40}$ (NaPW) showed similar characteristic peak position except that the peaks of salts shifted by 1–2° to higher diffraction angles (Fig. 1b). The XRD results of KPW (not shown) were similar to that of NaPW. For the fresh HPW/Cs–Nb catalyst, no obvious characteristic peaks of bulk HPW were observed with HPW loading up to 50%, indicating that HPW was well dispersed on the Cs-modified Nb_2O_5 [6]. The HPW/Cs–Nb catalyst was stable and showed similar XRD results before and after reaction with pure glycerol in (Figs. 1c, 1b) [6]. However, the peaks shifted to higher diffraction angles after 30 h of reaction with plant crude glycerol compared with the fresh HPW/Cs–Nb (Fig. 1*d*). Similar behavior was observed on HPW/Cs-Nb after 30 h of reaction with synthetic crude glycerol with Na^+ and K^+ (Figs. 1*f*, 1*g*). The change in diffraction angles was similar for the NaPW, indicating the neutralization by the alkali metal ions during the dehydration reaction. The Na^+ or K^+ salts of 12-tungstophosphoric acid were formed without destruction of the Kegging anion structure [24–26].

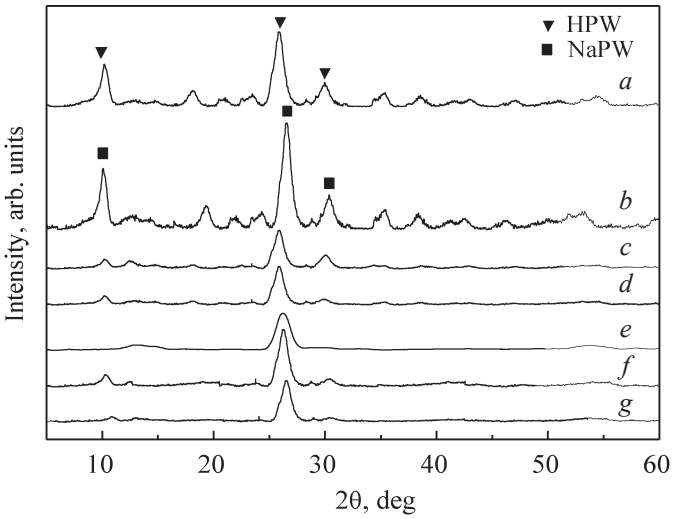

Fig. 1. XRD patterns of (*a*) HPW, (*b*) NaPW, (*c*) fresh HPW/Cs–Nb, (*d*) HPW/Cs–Nb after 30 h reaction with pure glycerol, (*e*) HPW/Cs–Nb after 30 h reaction with plant crude glycerol, and HPW/Cs–Nb after 30 h reaction with synthetic crude glycerol containing (*f*) Na^+ and (7) K^+.

Catalyst acidity. The NH_3-TPD was conducted with the fresh and used HPW/Cs–Nb catalysts to characterize the acidity properties. The Na^+–HPW/Cs–Nb catalysts were also examined to investigate the influence of alkali metal ions on the catalysts. The desorption temperature of NH_3 was used to classify the acid sites into weak (100–300°C), medium (300–500°C), and strong (>500°C) sites [27, 28]. The results are listed in Table 2. All the NH_3-TPD profiles displayed one or more wide peaks from 100 to 600°C. For bulk HPW, the strong acid sites caused coke formation in the glycerol dehydration and had limited thermal stability. For HPW/Cs–Nb, a large amount of strong acid sites were converted to medium acid sites by both HPW dispersion and Cs neutralization, in consistent with the results of Haider and Wang [29–31]. The fresh HPW/Cs–Nb catalyst showed the largest amount of acid sites with 12% weak acid sites, 78% medium acid sites, and 10% strong acid sites. The acidity amount and distribution of HPW/Cs–Nb after 30 h conversion of pure glycerol was very similar to that of the fresh catalyst, confirming that the HPW/Cs–Nb catalyst had good stability. After reaction with plant crude glycerol, however, the ratio of weak acidity on HPW/Cs–Nb increased to 68%.

After the reaction with synthetic crude glycerol containing organic impurities, the catalyst showed no obvious change compared with the fresh catalyst. However, with the synthetic crude glycerol containing Na^+ and K^+, a large amount of medium acid sites converted to weak acid sites due to the over neutralization of protonic sites by reaction between the alkli metal ions and Keggin anion. The total amount of acid sites also decreased. This phenomenon was also observed by Corma et al. [24, 26, 32] on Cs^+, Li^+, and NH_4^+ neutrilization of 12-tungstophosphoric acid. The influence of the alkali metal ions on the catalyst acid properties was similar for Na^+ and K^+. Therefore, the Na^+–HPW/Cs–Nb catalyst was used to further confirm the influence of the alkali metal ions. After Na^+ neutralization, the strong and medium acid sites on HPW were converted to weak ones. There were 71% weak acid sites and 21% medium acid sites on 5Na^+–HPW/Cs–Nb. The fraction of weak acid sites further increased to 84% when the Na^+ amount increased to 10%. The total amount of acid sites also decreased on Na^+–HPW/Cs–Nb.

The types of the surface acid sites were characterized by FTIR of pyridine. According to the literature, the bands at 1535–1545 and 1445–1460 cm^{-1} are characteristic of

Table 2 Acidic properties of the glycerol dehydeaion catalysts

Catalyst	Acidity [mmol NH_3/g][c]					
	Weak		Medium		Strong	
Nb_2O_5	0.02	81%	0.01	19%	0.00	0%
HPW/Cs–Nb	0.09	12%	0.69	78%	0.20	10%
HPW/Cs–Nb(pure)[a]	0.15	20%	0.64	72%	0.16	8%
HPW/Cs–Nb (plant crude)	0.41	68%	0.17	24%	0.13	8%
HPW/Cs–Nb (methanol)[b]	0.12	15%	0.63	72%	0.25	12%
HPW/Cs–Nb (FFA)	0.13	17%	0.64	74%	0.19	10%
HPW/Cs–Nb (FAME)	0.10	13%	0.60	74%	0.24	13%
HPW/Cs–Nb (glycerides)	0.15	19%	0.64	72%	0.19	9%
HPW/Cs–Nb(Na^+)	0.40	66%	0.16	23%	0.19	11%
HPW/Cs–Nb (K^+)	0.42	67%	0.19	26%	0.11	7%
5Na^+–HPW/Cs–Nb	0.37	71%	0.13	21%	0.11	8%
10Na^+–HPW/Cs–Nb	0.34	84%	0.08	16%	0.01	1%

[a] HPW/Cs-Nb(pure)/(plant crude) was the catalyst after 30h conversion of pure or plant crude glycerol to acrolein.
[b] HPW/Cs-Nb(methanol)/(FFA)/(FAME)/(glycerides)/(Na^+)/(K^+) was the catalyst after 30h conversion of synthetic crude glycerol to acrolein.
[c] Desorption temperature: weak 100–300°C ; medium 300–500°C ; strong > 500°C.

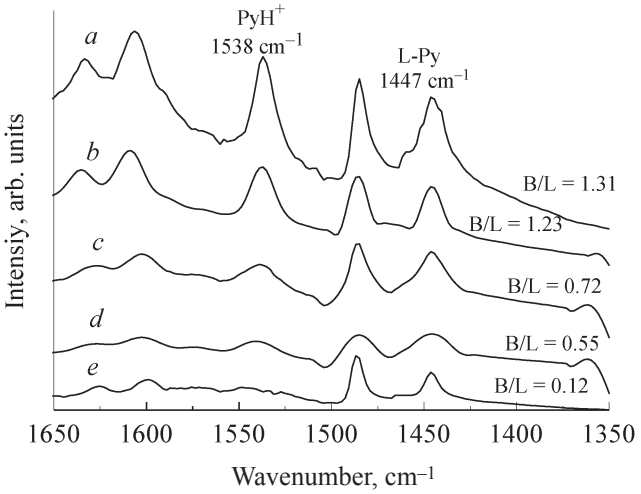

Fig. 2. IR spectra of pyridine adsorbed on (a) Fresh HPW/Cs-Nb, (b) HPW/Cs–Nb after 30 h reaction with pure glycerol, (c) HPW/Cs-Nb after reaction with plant crude glycerol, (d) 5Na^+–HPW/Cs-Nb and (e) 10Na^+–HPW/Cs-Nb before reaction.

Brønsted (PyH^+) and Lewis (PyL) acid sites, respectively, and the bands at 1480–1490 cm^{-1} belong to hydrogen-bonded pyridine (hb-Py) [33–35]. As shown in Fig. 2a, the HPW/Cs–Nb catalyst showed Brønsted acidity at 1538 cm^{-1}. The effective Brønsted acid sites were well maintained on the catalyst after reaction with pure glycerol, as shown in Fig. 2b. The amount of both Brønsted and Lewis acid sites decreased after reaction with synthetic crude glycerol containing Na^+, and the amount of Brønsted acid sites decreased more significantly. Figure 2 also shows the ratio between the Brønsted and Lewis acid sites (B/L), which was defined as the ratio of the peak areas at 1540 and 1450 cm^{-1} in the FTIR spectra. The B/L value remained similar on the used catalyst after 30 h of reaction with pure glycerol in Fig. 2b. However, after reaction with plant crude glycerol the B/L value of the used catalyst decreased to 0.72 (Fig. 2c). The B/L was 0.55 and 0.12 for the fresh Na^+–HPW/Cs–Nb catalysts with Na^+ loading of 5 and 10% in Figs. 2d and 2e, respectively, which was much lower than B/L = 1.3 on fresh HPW/Cs–Nb.

Influence of Impurities on Glycerol Dehydration-Oxidation

Glycerol dehydration-oxidation with different feedstocks. The aqueous solutions of pure glycerol, plant crude glycerol, and synthetic crude glycerol containing one typical impurity were tested for comparison. The reaction results are shown in Table 3 and Fig. 3.

With pure glycerol, the conversion of glycerol was 100% and the selectivity to acrylic acid was 81–83%

Table 3 Reaction results of the different glycerol[a]

Feed[b]	X[c], mol %	Production selecivity (mol%)			
		acrylic acid route		acetic acid route	
		acrylic acid	total[d]	acetic acid	total
Aqueous glycerol	100	85	87	4	4
Plant crude glycerol	95	73	78	15	17
Synthetic crude glycerol (methanol)	100	85	86	6	7
Synthetic crude glycerol (FFA)	100	84	85	5	7
Synthetic crude glycerol (FAME)	100	83	87	5	6
Synthetic crude glycerol (glycerides)	100	84	85	6	7
Synthetic crude glycerol (Na^+)	90	75	77	14	16
Synthetic crude glycerol (K^+)	89	76	76	13	14

[a] Reaction conditions: 300°C, 0.50 g 20CsPW–Nb, 0.5 g VMo–SiC, 40 mL min^{-1} gas flow rate (O_2 = 6 mL min^{-1}), 20 wt% glycerol solution fed at 0.6 mL h^{-1} (0.24 h^{-1} glycerol WHSV), TOS of 10 h.

[b] Glycerol-impurity is the 20 wt % aqueous solution of synthetic crude glycerol containing 5 wt % impurity (methanol, methyl stearate, NaCl or KCl)

[c] X is the conversion of glycerol.

[d] The selectivities of the acrylic acid route and acetic acid route were calculated by summing up the selectivities of the main products on Brønsted acid sites and Lewis acid sites.

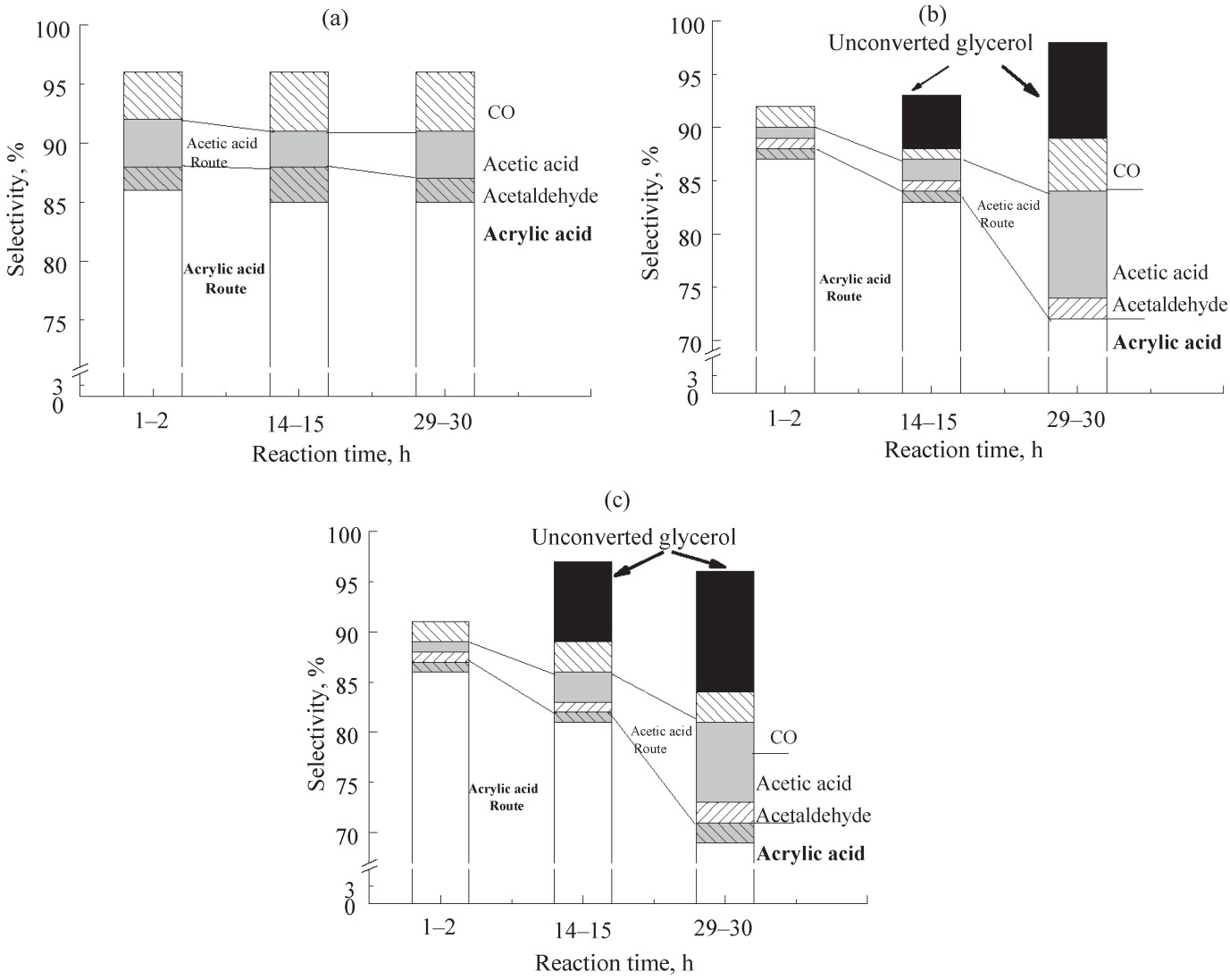

Fig. 3. Catalyst stability and product distribution for (a) pure glycerol, synthetic crude glycerol with (b) Na^+ and (c) K^+.

at TOS of 30 h over 50HPW/Cs-Nb, and the product distribution was stable during the whole reaction time in Fig. 3a. When the plant crude glycerol containing 3.4 wt % K^+ and 0.42 wt % Na^+ was fed in to the reactor, fast deactivation was observed and the acrylic acid selectivity decreased to 65% with 13% unconverted glycerol after 30 h, as listed in Table 3. Several kinds of synthetic crude glycerol with methanol, methyl stearate or alkli metal ions were prepared and used to study the influence of different impurities on the product distribution. As shown in Table 3, the selectivity to acrylic acid was 83–85% and the glycerol conversion was 100% when using synthetic crude glycerol containing methanol and methyl stearate, indicating that these organic impurities had no influence on the activity and selectivity of the dehydration–oxidation system. When using synthetic crude glycerol containing Na^+ or K^+, the dehydration–oxidation system had poor stability, as shown in Figs. 3b and 3c. The initial selectivity to acrylic acid was still as high as 87%, but significant deactivation was observed at TOS = 30 h with 15–17% decrease in the glycerol conversion. The activity decreased due to the deposition of alkli metal ions on the dehydration catalyst and the decrease in total amount of acid sites.

The alkali metal ions affected the product yield by changing the selectivity of different dehydration–oxidation routes, which was proposed in Scheme 1. According to previous study, the formation of acrolein occurs on

Scheme 1. The proposed overall reaction pathways for the glycerol dehydration and subsequent oxidation on Brønsted and Lewis acid site.

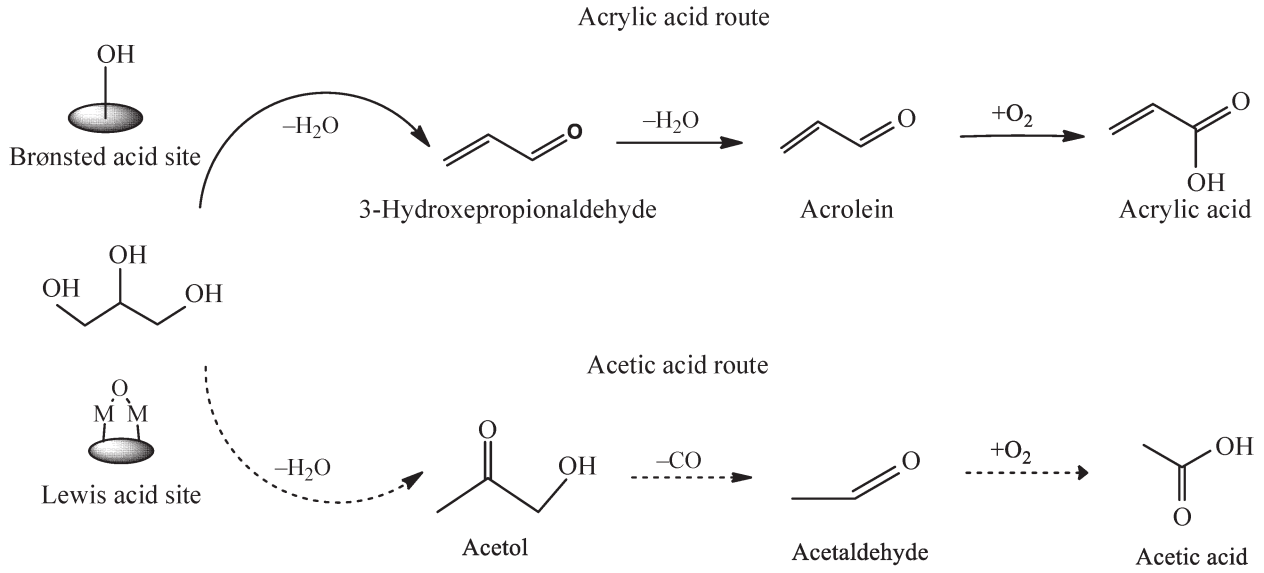

Brønsted acid sites. The 3-hydroxypropionaldehyde is produced by the first dehydration step and acrolein by the second, which in turn is converted to acrylic acid by the dehydration–oxidation step [7, 36]. On the Lewis acid sites, the dehydration–oxidation reaction produces acetic acid and acetaldehyde. Table 3 shows the total product selectivity of the acrylic acid route on Brønsted acid sites (acrylic acid and acrolein) and that of the acetic acid route on Lewis acid sites (acetic acid and acetaldehyde). When the aqueous pure glycerol was used, the selectivities of the acrylic acid and acetic acid routes were 87 and 4%, respectively. When the plant crude glycerol was used, the selectivity of acrylic acid routes decreased to 78% and that of the acetic acid route increased to 17%. This was caused by the decreased amount of Brønsted acid sites and B/L ratio in Fig. 2c. The results on synthetic crude glycerol showed that the product distribution was insensitive to methanol and FFA, but was significantly affect by Na^+. When Na^+ were added to the glycerol solution, the selectivity of the acetic acid route increased to 5% at TOS =15 h and 12% at TOS = 30 h (Fig. 3b). The major byproducts were acetic acid (11%), acetaldehyde (2%), and some CO_x. At the same time the selectivity of the acrylic acid route decreased to 82% at TOS =15 h and 72% at TOS = 30 h. Similar phenomenon was observed with addition of K^+, as shown in Fig. 3c.

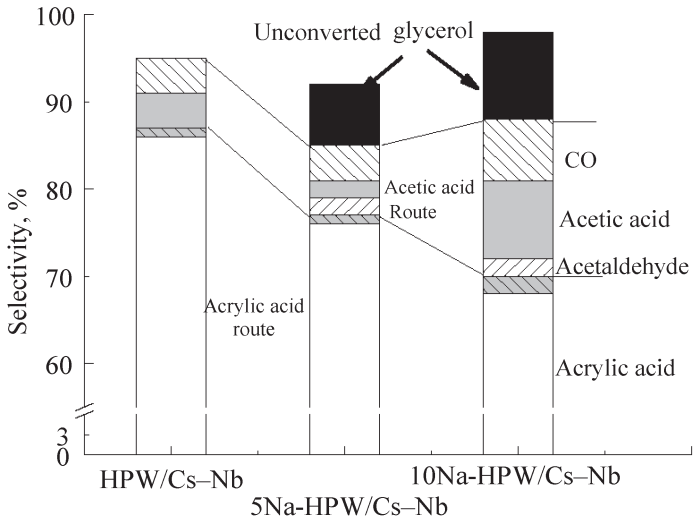

Fig. 4. Effect of Na^+ loading on the product selectivity after 30 h reaction with pure glycerol

Glycerol dehydration–oxidation over Na^+–HPW/Cs–Nb and VMo–SiC. Note that only the synthetic crude glycerol containing alkali metal ions caused dehydration catalyst deactivation and the effect of Na^+ and K^+ were very similar. Further experiments using Na^+–HPW/Cs–Nb for dehydration and VMo–SiC for oxidation with pure glycerol were carried out to confirm that the alkali metal ions were the main reason for the loss of catalyst activity and decrease in selectivity when using crude glycerol. The effect of Na^+ loading on the product selectivity with pure glycerol was shown in Fig. 4.

The 50HPW/Cs*Nb and VMo–SiC catalyst showed 87% acrylic acid selectivity and complete glycerol

conversion after 30 h. Both the glycerol conversion and the yield of acrylic acid decreased with increasing loading of Na^+. There was 8–13% unconverted glycerol over the dehydration–oxidation system as a result of decreased amount of the acid sites on the dehydration catalyst. Only 70% yield of acrylic acid was achieved on $5Na^+$–HPW/Cs–Nb and VMo–SiC system. The yield of acrylic acid further decreased to 57% on $10Na^+$–HPW/Cs–Nb and VMo–SiC system. The loading of Na^+ also affected the selectivity of the reaction route by decreasing the B/L value of the dehydration catalyst in Figs. 2d, 2e. The HPW/Cs–Nb catalyst had the highest value of B/L and 87% selectivity of the acrylic acid route. In contrast, the selectivity of the acrylic acid route decreased by 12% over $5Na^+$–HPW/Cs–Nb and by 20% over $10Na^+$–HPW/Cs–Nb, as shown in Fig. 4. At the same time, the selectivity of the acetic acid route increased due to the formation of acetic acid, acetaldehyde and CO_. These results further confirmed that the Na^+ and K^+ impurity in the crude glycerol was the major factor that decreased the glycerol conversion and acrylic acid yield.

Catalytic Results of Desalted Glycerol Dehydration-Oxidation

In order to increase the stability of dehydration–oxidation system during the catalytic conversion of plant crude glycerol, the alkali metal ions were removed by glycerol desalination with ion exchange resin. Figure 5 shows the glycerol conversion and product selectivity as a function of the reaction time with 20 wt % aqueous solution of plant crude glycerol and desalted crude glycerol at 300°C. It can be seen that the glycerol conversion decreased from 100 to 89% and the acrylic acid selectivity decreased from 88 to 71% after 40 h of reaction with plant crude glycerol. In comparison, the acrylic acid yield was kept stable at 87% when desalted crude glycerol was used, which was similar to that with pure glycerol. To investigate the thermal stability of the catalyst for desalted glycerol dehydration, the reaction was carried out after 3 h regeneration of the catalyst at 500°C in the air. The dehydration–oxidation system showed good thermal stability and gave the same activity and selectivity as before regeneration. These results showed that it was feasible to use desalted crude glycerol to efficiently produce acrylic acid. Because the desalination process was much cheaper than the whole purification process for refined glycerol production, this approach significantly enhanced the competitiveness of acrylic acid production from glycerol.

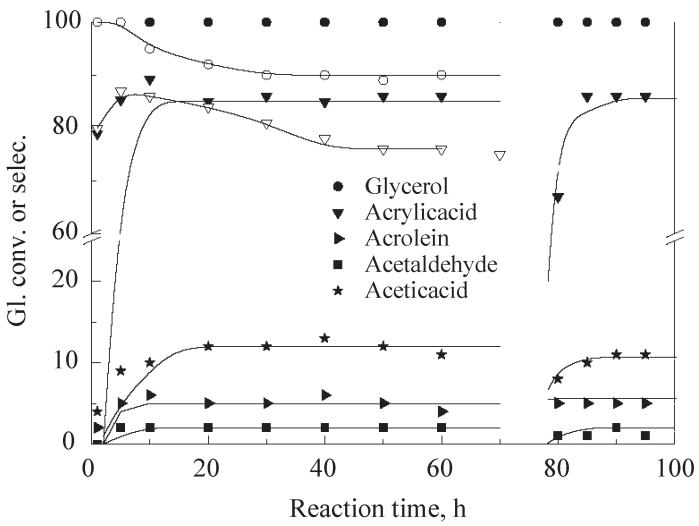

Fig. 5. Variation of glycerol conversion and product selectivity with the reaction time with 20 wt% plant crude glycerol (open symbol) and desalted crude glycerol (closed symbol) at 300°C before and after in situ regeneration at 500°C for 3 h.

CONCLUSIONS

The feasibility of using crude glycerol as feedback for the acrylic acid production by dehydration-oxidation system was explored in this work. When using crude glycerol for dehydration to acrylic acid, the dehydration–oxidation system showed good resistance to organic impurities such as methanol and fatty acid. But the alkaline metal ions such as Na^+ and K^+ converted the medium acid sites on the dehydration catalyst to weak acid sites and significantly decreased the yield of acrylic acid. Among all the impurities, only the alkaline metal ions need to be removed before the dehydration–oxidation reaction. After desalination of the plant crude glycerol with ion-exchange resin, the catalyst gave 86% acrylic acid yield, which was as high as that with pure glycerol. No deactivation was observed with the system for at least 70 h. Both catalysts had good thermal stability at the coke burning temperature of 500°C, and the activity and selectivity were the same as those before the regeneration process. Our work provides a green and efficient route to produce acrylic acid from crude glycerol, which is a promising alternative and complement to the petroleum-based production of acrylic acid due to its economic and environmental benefits.

REFERENCES

1. Xia, S.X., Zheng, L.P., Nie, R.F., Chen, P., Lou, H., and Hou, Z.Y., *Chin J. Catal.*, 2013, vol. 34, pp. 986–992.
2. Volkov, S.V., Khar'kova, L.B., Fokina, Z.A., et al., *Russ. J. Appl. Chem*., 2007, vol. 80, pp. 193–200.
3. Hu, J.Y., Liu, X.Y., Fan, Y.Q., Xie, S.H., Pei, Y., Qiao, M.H., Fan, K.N., Zhang, X.X., Zong, B.N., *Chin J Catal* , 2013, vol. 34, pp. 1020–2026.
4. Katryniok, B., Paul, S., Belliere-Baca, V., Rey, P., and Dumeignil, F., *Green Chem.*, 2010, vol. 12, pp. 2079–2098.
5. Ma, J.P., Yu, W.Q., Wang, M., Jia, X.Q., Lu, F., and Xu, J., *Chin J. Catal.*, 2013, vol. 34, pp. 492–507.
6. Cheng, L., Liu, L., and Ye, X.P., *Oil Chem. Soc.*, 2013, vol. 90, pp. 601–610.
7. Volkov, S.V., Khar'kova, L.B., Baranets, S.A. et al., *Russ J Appl Chem.,* 2016, vol. 89, pp. 233–237.
8. Witsuthammakul, A. and Sooknoi, T., *Appl. Catal. A*, 2012, vol. 413, pp. 109–116.
9. Jekewitz, T., Blickhan, N., Endres, S., Drochner, A., and Vogel, H., *Catal. Commun.*, 2012, vol. 20, pp. 25–28.
10. Chieregato, A., Basile, F., Concepción, P., Guidetti, S., Liosi, G., Soriano, M.D., Trevisanut, C., Cavani, F., Nieto, J.M.L., Deleplanque, J., Dubois, J.-L., Devaux, J.-F., and Ueda, W., *Catal. Today*, 2012, vol. 197, pp. 58–65.
11. Xiao, Y., Xiao, G., and Varma, A., *Ind. Eng. Chem. Res.*, 2013, vol. 52, pp. 14291–14296.
12. Liu, R., Wang, T., Liu, C., and Jin, Y., *Chin. J. Catal.*, 2013, vol. 34, pp. 2174-2182.
13. Liu, R., Wang, T., and Jin, Y., *Catal. Today*, 2013, vol. 233, pp. 127–132
14. Konaka, A., Tago, T., Yoshikawa, T., Shitara, H., Nakasaka, Y., and Masuda, T., *Ind. Eng. Chem. Res.*, 2013, vol. 52, pp. 15509-15515.
15. Hu, S., Luo, X., Wan, C., and Li, Y., *J. Agric. Food Chem.*, 2012, vol. 60, pp. 5915–5921.
16. Yadav, G.D.. Sharma. R.V.. and Katole, S.O.. *Ind. Eng. Chem. Res.*, 2013, vol. 52, pp. 10133–10144.
17. Cheng, L., Liu, L., and Ye, X.P., *J. Chem. Technol. Biotechnol.*, 2013, vol. 90, pp. 601–610.
18. Zhang, M., Li, A., Zhou, Q., Shuang, C., Zhou, Y., and Wang, M., *Ind. Eng. Chem. Res.*, 2014, vol. 53, pp. 340–345.
19. Carmona, M., Lech, A., de Lucas, A., Perez, A., and Rodriguez, J.F., *J. Chem. Technol. Biotechnol.*, 2009, vol. 84, pp. 1130-1135.
20. Carmona, M., Warchol, J., de Lucas, A., and Rodriguez, J.F., *J. Chem. Technol. Biotechnol.*, 2008, vol. 53, pp. 1325–1331.
21. Wisniewski, L., Pereira, C.S.M., Polakovic, M., and Rodrigues, A.E., *Adsorption*, 2014, vol. 20, pp. 483–492.
22. Zheng, Y., Tang, Q., Wang, T., Liao, Y., and Wang, J., *Chem. Eng. Technol.,* 2013, vol. 36, pp. 1951–1956.
23. Lakeev, S.N., Maydanova, I.O., Mullakhmetov, R.F., et al., 2016, vol. 89, pp. 1–15.
24. Carmona, M., Valverde, J.L., Perez, A., Warchol, J., and Rodriguez, J.F., *J Catal.*, 2009, vol. 84, pp. 738–744.
25. Pizzio, L.R. and Blanco, M.N., *Appl. Catal., A*, 2003, vol. 255, pp. 265–277.
26. Yoshimune, M., Yoshinaga, Y., and Okuhara, T., *Microporous Mesoporous Mate.*, 2002, vol. 51, pp. 165–174.
27. Corma, A. Martinez, Martinez, C., Hayashi, H., and Moffat, J.B., *J. Catal.*, 1996, vol. 164, pp. 422–432.
28. Katryniok, B., Paul, S., Capron, M., Lancelot, C., Belliere-Baca, V., Rey, P., and Dumeignil, F., *Green Chem.*, 2010, vol. 12, pp. 2273–2273.
29. Shen, L., Feng, Y., Yin, H., Wang, A., Yu, L., Jiang, T., Shen, Y., and Wu, Z., *J. Ind. Eng. Chem.*, 2011, vol. 17, pp. 484–492.
30. Haider, M.H., Dummer, N.F., Zhang, D., Miedziak, P., Davies, T.E., Taylor, S.H., Willock, D.J., Knight, D.W., Chadwick, D., and Hutchings, G.J., *J. Catal*, 2012, vol. 286, pp. 206–213.
31. Yang, W., Billy, J., Taarit, Y.B., Vedrine, J.C., and Essayem, N., *Catal. Today*, 2002, vol. 73, pp. 153–165.
32. Choi, S.M., Wang, Y., Nie, Z.M., Liu, J., and Peden, C., *Catal. Today*, 2000, vol. 55, pp. 117–124.
33. Haber, J., Matachowski, L., Mucha, D., Stoch, J., and Sarv, P., *Inorg. Chem.*, 2005, vol. 44, pp. 6695–6703.
34. Corma, A., *Chem Rev.*, 1995, vol. 95, pp. 559–614.
35. Emeis, C.A., Kalevaru, V.N., Benhmid, A., Radnik, J., Pohl, M.M., Bentrup, U., and Martin, A., *J. Catal.*, 1993, vol. 141, pp. 347–354.
36. Kalevaru, V.N., Benhmid, A., Radnik, J., Pohl, M.M., Bentrup, U., and Martin, A., *J. Catal.*, 2007, vol. 246, pp. 399-412.